Chimera distribution amplitudes for the pion and the longitudinally polarized ρ-meson

N. G. Stefanis[1,*] and A. V. Pimikov[2,3,†]

[1] *Institut für Theoretische Physik II, Ruhr-Universität Bochum, D-44780 Bochum, Germany*
[2] *Bogoliubov Laboratory of Theoretical Physics, JINR, 141980 Dubna, Russia*
[3] *Institute of Modern Physics, Chinese Academy of Sciences, Lanzhou, 730000, P. R. China*

(Dated: January 21, 2022)

Using QCD sum rules with nonlocal condensates, we show that the distribution amplitude of the longitudinally polarized ρ-meson may have a shorttailed platykurtic profile in close analogy to our recently proposed platykurtic distribution amplitude for the pion. Such a chimera distribution de facto amalgamates the broad unimodal profile of the distribution amplitude, obtained with a Dyson–Schwinger equations-based computational scheme, with the suppressed tails characterizing the bimodal distribution amplitudes derived from QCD sum rules with nonlocal condensates. We argue that pattern formation, emerging from the collective synchronization of coupled oscillators, can provide a single theoretical scaffolding to study unimodal and bimodal distribution amplitudes of light mesons without recourse to particular computational schemes and the reasons for them.

PACS numbers: 12.38.Lg, 12.38.Bx, 14.40.Be, 05.45.Xt

arXiv:1506.01302v5 [hep-ph] 27 Oct 2016

I. INTRODUCTION

Many theoretical models exist to describe the valence parton distribution amplitude (DA) of the π, the ρ (both longitudinally and transversally polarized), and other mesons. In particular the pion, the lightest bound state within Quantum Chromodynamics (QCD), provides a suitable "laboratory" for testing new ideas and techniques to catch the main ingredients of the underlying quark-gluon dynamics entering exclusive QCD processes (see [1–3] for reviews). In this paper we will present an amplification of the recent analysis by one of us in [4], continued in [5], for the pion and consider its extension to the longitudinally polarized ρ meson ($\rho_\parallel$). The new mode of thought in [4] is based on the ubiquitous phenomenon of synchronization (Sync for short) in complex systems and we will expand the status of this subject towards a deeper understanding of the meson DAs. In this way, we will redetermine the $\rho_\parallel$ DA using QCD sum rules with nonlocal condensates (NLC) within the approach developed in [6–8].

Our primary findings to be discussed later can be summarized as follows: First, we provide more details about the structure of the Sync-inspired shorttailed (i.e., endpoint-suppressed) platykurtic (pk) π DA, proposed in [4], and quantify the uncertainties of its expansion coefficients. This DA is a kind of chimera[1] state because it mimics within the NLC-based approach characteristics pertaining to the dynamical chiral symmetry breaking (DCSB) described in terms of Dyson–Schwinger equations (DSE) [9, 10]. In particular it conserves NLC-generated endpoint suppression of the π DA combining it with a broad downward concave shape in the central region. Second, using similar mathematical techniques, we obtain within the reliability range of the NLC approach a regime of DAs for the $\rho_\parallel$ meson characterized by a shorttailed platykurtic profile. Third, we employ statistical measures, like the kurtosis, to classify meson DAs with respect to their peakedness relative to the tail flatness and heaviness.

The rest of the paper is organized as follows. The next two sections (Sec. II and Sec. III) discuss the theoretical basis for the description of meson DAs within QCD. Section IV sketches the derivation of the π and $\rho_\parallel$ DAs from QCD sum rules with NLCs. We will then proceed to investigate how meson DAs can be analyzed in terms of synchronization concepts (Sec. V). Synthetic meson DAs will be considered in Sec. VI, where also the important chimera DAs with a shorttailed platykurtic profile will be presented. Finally, Sec. VII will be reserved for the summary of our main results and conclusions.

II. MESON DAs IN QCD

Let us consider the pion DA, starting with its definition. [2] Applying collinear factorization in QCD, the π DA of leading-twist two, $\varphi_\pi^{(2)}(x,\mu^2)$, encodes the distribution of the longitudinal momentum of the pion between its two valence constituents: the quark and the antiquark, with corresponding longitudinal-momentum fractions $x_q = x = (k^0+k^3)/(P^0+P^3) = k^+/P^+$ and $x_{\bar q} = 1-x \equiv \bar x$, respectively. Its momentum-scale dependence stems from the renormalization of the current

*Electronic address: stefanis@tp2.ruhr-uni-bochum.de
†Electronic address: pimikov@theor.jinr.ru

[1] An imaginary creature in Greek mythology made up of different animals.

[2] The exposition to follow relies upon the review in [3] to which we refer for details and the original references.

operator in

$$\langle 0|\bar{q}(z)\gamma_\mu\gamma_5[z,0]q(0)|\pi(P)\rangle|_{z^2=0} = if_\pi P_\mu \int_0^1 dx e^{ix(z\cdot P)} \times\varphi_\pi^{(2)}\left(x,\mu^2\right), \quad (1)$$

where the gauge link $[z,0] = \mathcal{P}\exp[-ig\int_0^z dw_\mu A_a^\mu(w)t_a] = 1$ is set equal to unity on account of the lightcone gauge $A\cdot n \equiv A^+ = 0$ ($n^2 = 0$). The pion DA is related to the Bethe–Salpeter wave function $\psi_\pi(x,k_\perp)$ by integrating over the transverse parton momentum $k_\perp$, i.e.,

$$\varphi_\pi^{(2)}\left(x,\mu^2\right) \sim \int^{k_\perp^2<\mu^2} d^2k_\perp \psi_\pi(x,k_\perp). \quad (2)$$

Because the dependence on the momentum scale of any meson DA is controlled by the Efremov-Radyushkin–Brodsky-Lepage (ERBL) [11, 12] evolution equation, each meson DA can be expressed in terms of the one-loop eigenfunctions of this equation, $\psi_n(x) = 6x(1-x)C_n^{(3/2)}(2x-1)$, with the asymptotic (asy) DA being given by $\varphi_\pi^{\rm asy}(x) = 6x(1-x) \equiv 6x\bar{x}$, and $C_n^{(3/2)}(2x-1)$ denoting the Gegenbauer polynomials of order 3/2 within the complete and orthonormal basis on $x \in [0,1]$ with respect to the weight $x\bar{x}$. Thus, one has the (scale-dependent) conformal expansion

$$\varphi_\pi^{(2)}(x,\mu^2) = \sum_{n=0,2,4,\ldots}^{\infty} a_n(\mu^2)\psi_n(x) \quad (3)$$

in terms of the nonperturbative coefficients $a_n(\mu^2)$. By virtue of the normalization condition $\int_0^1 dx\varphi_\pi^{(2)}(x,\mu^2) = 1$, $a_0 = 1$ at any scale μ^2.

III. GEGENBAUER DA REPRESENTATIONS

In our approach [6], based on QCD sum rules with nonlocal condensates [13–18], we calculated the moments

$$\langle\xi^N\rangle_\pi \equiv \int_0^1 dx(2x-1)^N\varphi_\pi^{(2)}(x,\mu^2) \quad (4)$$

up to $N = 10$ together with their intrinsic theoretical uncertainties at the typical hadronic scale $\mu^2 \approx 1.35$ GeV^2 [6]. Detailed estimates of the moment uncertainties can be found in [19, 20] (see also Table I)). This scale represents the average value of the Borel parameter M^2 in the stability window of the sum rule, notably, $M^2 \sim [m_\rho^2, s_0]$, where s_0 is the continuum threshold and m_ρ is the physical mass of the ρ meson. Note that the moments $\langle\xi^N\rangle_\pi$ coincide by construction with the central moments

$$\mu_N[\varphi_\pi] = \int_0^1 dx(x-\mu[\varphi_\pi])^N\varphi_\pi(x) = 2^{-N}\langle\xi^N\rangle_\pi \quad (5)$$

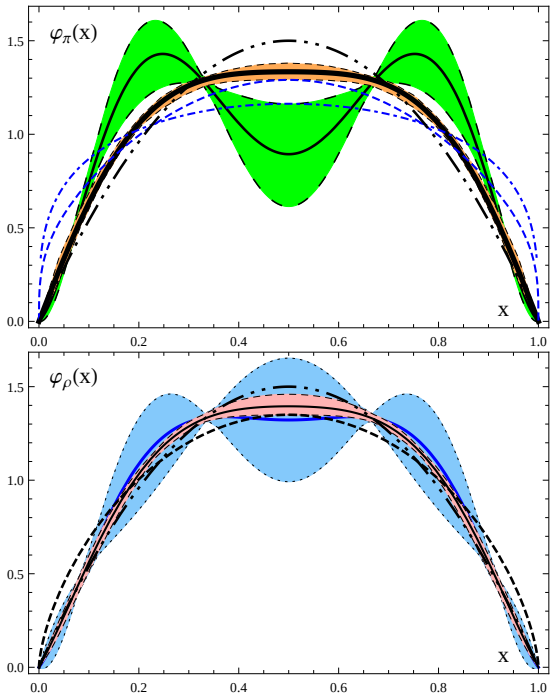


FIG. 1: (color online). The upper panel shows some characteristic pion DAs. The larger shaded (green) area displays the region of the bimodal Bakulev-Mikhailov-Stefanis (BMS) family of DAs derived in [6] from QCD sum rules with NLCs using the nonlocality parameter $\lambda_q^2 = 0.4$ GeV^2, defind in Sec. III. The family of the π platykurtic DAs is shown as a narrow shaded strip in red color, obtained with $\lambda_q^2 = 0.45$ GeV^2 at the edge of the NLC regime. The solid lines within both regions denote, respectively, the BMS model from [6] and the pk DA discussed in the text and in [4, 5]. The broken lines show the unimodal DSE-DB DA (dashed), the DSE-RL DA (dashed-dotted) (both from [9]), and the asymptotic DA (dashed-dotted-dotted). The lower panel illustrates various $\rho_\parallel$ DAs. The larger blue shaded area contains the family of DAs obtained in [8] using QCD sum rules with NLCs and $\lambda_q^2 = 0.4$ GeV^2, while the narrower strip in its interior indicates the platykurtic regime of these DAs. The solid lines within each band denote, respectively, the bimodal DA from [8] (lowest (blue) solid line) and the platykurtic DA (upper solid line) derived in this work. The lower dashed line represents the DA obtained from the DSE approach [10], whereas the dashed-dotted-dotted line displays again the asymptotic DA. All DAs in both panels refer to the scale $\mu^2 = 4$ GeV^2 after two-loop ERBL evolution, provided the initial proprietary scale was lower than this.

of $\varphi_\pi(x)$, where

$$\mu[\varphi_\pi] = \int_0^1 dx x\varphi_\pi(x) = \frac{1}{2} \quad (6)$$

is the mean of the DA. Using standard techniques (see, for example, [1, 3]), we extracted from the moments the corresponding conformal coefficients a_n entering Eq. (3). These quantities contain nonperturbative information and implicitly depend on the finite virtuality of the vacuum quarks, the latter expressed by means of the

nonlocality parameter $\lambda_q^2 = \langle\bar{q}igG^{\mu\nu}\sigma_{\mu\nu}q\rangle/2\langle\bar{q}(0)q(0)\rangle \approx [0.35-0.45]$ GeV^2. It was found that the first two coefficients (see Appendix C in [21])

$$a_2 = \frac{7}{12}\left(5\left\langle\xi^2\right\rangle - 1\right), \tag{7}$$

$$a_4 = \frac{77}{8}\left(\left\langle\xi^4\right\rangle - \frac{2}{3}\left\langle\xi^2\right\rangle + \frac{1}{21}\right) \tag{8}$$

dominate. Their values have been calculated with controlled accuracy in [6]. They read $a_2(\mu^2 \approx 1\ \text{GeV}^2) = 0.20$ and $a_4(\mu^2 \approx 1\ \text{GeV}^2) = -0.14$, whereas the next higher coefficients were computed in the same work as well and found to be much smaller, viz., $a_6 \approx a_2/3$; $a_8 \approx a_2/4$; $a_{10} \approx a_2/5$, but bearing large uncertainties. Their inclusion can add refinements to the method, as we have discussed in [22]. This apparent hierarchy, with each subsequent coefficient becoming smaller with the order of the conformal expansion, is not following from general principles; it is an inherent element of our specific approach. Indeed, one can even have an inverse ordering of the coefficients a_n — see [23] for such DAs. In the final analysis, the pion DA at the scale $\mu^2 \gtrsim 1$ GeV^2 can be written in the form ($\xi \equiv 2x-1 = x-\bar{x}$)

$$\varphi_\pi^{\rm BMS}(x) = 6x\bar{x}\left[1 + a_2 C_2^{(3/2)}(\xi) + a_4 C_4^{(3/2)}(\xi)\right], \tag{9}$$

where the label means Bakulev, Mikhailov, Stefanis [6]. This simple model probably offers a biased picture of the pion structure but its chief predictions are in good agreement with measurements and various lattice simulations, as detailed in a series of papers [5–7, 20–22, 24–29]. The reason is that physical observables, like the pion-photon transition or the pion's electromagnetic form factor are given in terms of integrals of the DAs with smooth coefficient functions. Because the leading-order anomalous dimensions of the involved operators in the matrix elements between the meson state and the vacuum are positive (except $\gamma_0 = 0$), the higher coefficients are logarithmically suppressed at large scales, so that only $\psi_0(x) = \varphi_\pi^{\rm asy}(x)$ survives. This is particularly visible in the inverse moment of the pion DA, cf. Eq. (13), in which the oscillating terms are washed out and strongly suppressed as the momentum increases. The profiles of the meson DAs, considered in this work, are shown in the upper (π) and the lower ($\rho_\parallel$) panel of Fig. 1, respectively.

To leading logarithmic accuracy, the conformal coefficients a_n are multiplicatively renormalizable and the anomalous dimensions are known in closed form, see, for example, [3]. At the next-to-leading-order (NLO) level, the momentum-scale dependence of the conformal coefficients (or moments) is more complicated owing to the mixing of the operators under renormalization [30–32]. The diagonal elements of the corresponding two-loop anomalous-dimension matrix coincide with the flavor nonsinglet anomalous dimensions known from deeply inelastic scattering. They have been computed in [33], corrected in [34], and verified in [35]. The NLO ERBL kernel was calculated in [36–38], while the analytic expressions for the mixing coefficients to obtain the corresponding eigenfunctions were given in [31, 32]. Bear in mind that the next-to-leading-order corrections under a change of scale using a running coupling appear as a two-loop contribution of the eigenvalues and as an α_s correction to the eigenfunctions. A detailed exposition of the ERBL evolution of the pion DA at the two-loop level, as used in the present work, is provided in Appendix D in [24].

It is convenient to employ another Gegenbauer representation ("Gegenbauer-α") proposed in [9, 10], notably,

$$\varphi_\pi^{(2)}(x,\mu^2) = f(\{\alpha, a_2^\alpha, ..., a_{j_s}^\alpha\}, x) = \psi_0^{(\alpha)}(x) + \sum_{j=2,4,...}^{j_s} a_j^\alpha(\mu^2)\psi_n^{(\alpha)}(x), \tag{10}$$

where

$$\psi_n^{(\alpha)}(x) = N_\alpha (x\bar{x})^{\alpha_-} C_n^{(\alpha)}(2x-1) \tag{11}$$

and $N_\alpha = 1/B(\alpha+1/2, \alpha+1/2)$, $\alpha_- = \alpha - 1/2$, where $B(x,y)$ is the Euler beta function. The Gegenbauer polynomials $C_n^{(\alpha)}(2x-1)$ form an orthonormal set over $x \in [0,1]$ with respect to the weight $[x\bar{x}]^{\alpha_-}$. The difference to the conformal expansion in Eq. (3) is that the order of the Gegenbauer polynomials is not a priori fixed to the value 3/2, but is allowed to vary in order to accelerate the reconstruction procedure of meson DAs on $x \in [0,1]$. However, expansion (10) is not directly amenable to ERBL evolution because the functions $\psi_n^\alpha(x)$ are not its eigenfunctions. To evolve $\varphi_\pi^{(2)}(x,\mu^2)$, expressed via (10), to another scale $Q^2 > \mu^2$, one has to project it first onto the conformal basis $\{\psi_n(x)\}$ and then determine α_- and a_j^α at the new scale. The authors of the works in Refs. [9, 10] find that it is sufficient to include only one coefficient in this expansion, namely, a_2^α, so that Eq. (10) reduces to

$$\varphi_\pi^{(\alpha)}(x,\mu^2) = N_\alpha (x\bar{x})^{\alpha_-}[1 + a_2^\alpha C_2^{(\alpha)}(x-\bar{x})]. \tag{12}$$

Below, we will use for our analysis both representations in parallel and present the results in the form (a_2, a_4) and $(N_\alpha, \alpha_-, a_2^\alpha)$. It is worth bearing in mind that broad DAs of the form $\varphi_\pi(x) \sim (x\bar{x})^{\alpha_-}$ are not well represented by Eq. (9) which only employs the first two conformal coefficients. To approximate such DAs with sufficient accuracy, one would have to include a large number of coefficients of order 50 or more, see, for example, [31].

IV. π AND $\rho_\parallel$ DAs FROM NLC QCD SUM RULES

In this section, we discuss the derivation of the $\rho_\parallel$ DA using QCD sum rules with nonlocal condensates within

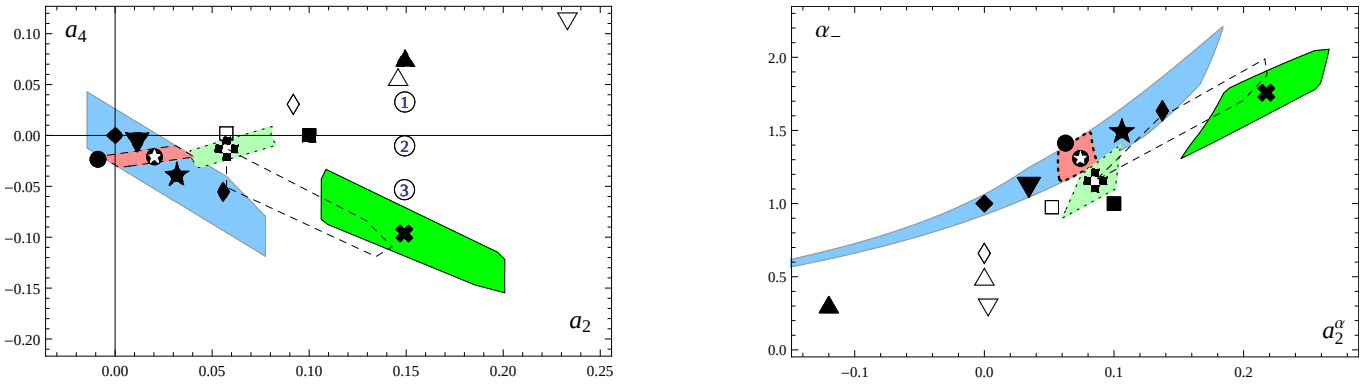


FIG. 2: (color online). Computed locations of various $\rho_\parallel$ and π DAs at $\mu^2 = 4$ GeV^2 in the plane spanned by the conformal coefficients a_2 and a_4 (left panel) and corresponding results in the plane (α_-, a_2^α) (right panel). The slanted (blue) rectangle further to the left shows the region of $\{a_2, a_4\}$ values obtained with NLC-QCD sum rules and $\lambda_q^2 = 0.4$ GeV^2 for the $\rho_\parallel$ DA in [8], with the smaller (red) rectangle in its interior denoting the platykurtic regime determined in this work. The other small (light-green) rectangle next to it contains the platykurtic region calculated for the pion DA in this work using $\lambda_q^2 = 0.45$ GeV^2 at the edge of the NLC regime. The larger slanted (green) rectangle further to the right contains the original values of $\{a_2, a_4\}$ for the pion DA obtained with $\lambda_q^2 = 0.4$ GeV^2 in [6]. The symbols ①, ②, and ③ show examples of synthetic DAs according to Eq. (26) for $a = 0.25$, $a = 0.5$, and $a = 0.75$, respectively. Corresponding results for the $\rho_\parallel$ DA at 4 GeV^2 in the (α_-, a_2^α) plane are displayed in the right panel with the following designations: The stretched (blue) strip shows the region of (α_-, a_2^α) values calculated with NLC-QCD sum rules and $\lambda_q^2 = 0.4$ GeV^2 in this work. The two smaller slanted rectangles illustrate the platykurtic regime for the $\rho_\parallel$ DA (upper red rectangle) and for the π DA (lower light-green rectangle); they correspond to the analogous graphs in the left panel. The other symbols in both panels denote the following DAs: ★ — bimodal $\rho_\parallel$ DA from NLC-QCD sum rules [8]; ♦ — bimodal $\rho_\parallel$ DA from NLC-QCD sum rules [18]; ✪ — platykurtic $\rho_\parallel$ DA (this work); ▼ — $\rho_\parallel$ DA from lightfront model [39]: ● — $\rho_\parallel$ DA from instanton model [40]; ■ — $\rho_\parallel$ DA from QCD sum rules [41]; □ — $\rho_\parallel$ DA from AdS/QCD [42] △ — π AdS/QCD [43]; ◊ — $\rho_\parallel$ DSE DA [10]; ◆ — asymptotic DA; ✖ (both panels) — BMS π DA [6]; ✜ (both panels) — platykurtic π DA; [4]; ▲ (both panels) — DSE-DB π DA [9]; ▽ (both panels) — DSE-RL π DA [9]. The slanted rectangles, bounded by dashed lines, in both panels display the regions determined in this work for the π DA using NLC QCD sum rules with $\lambda_q^2 = 0.45$ GeV^2. When the proprietary scale of the studied DAs was different from 2 GeV, NLO evolution was applied to determine their coefficients at this scale. The numerical values of all coefficients are given in Table I.

the scheme developed in [6–8]. The main conceptual idea is to apply the sum-rule method in combination with vacuum averages of nonlocal operators [13–18]. Following this rationale, one can determine the moments $\langle \xi^N \rangle$ of a meson DA using a sum rule with nonlocal condensates. In addition, due to the absence of endpoint singularities in the NLC approach, one is able to calculate the inverse moment

$$\langle x^{-1} \rangle_\pi \equiv \int_0^1 dx x^{-1} \varphi_\pi(x) \tag{13}$$

via an independent sum rule at the same low renormalization scale $\mu \gtrsim 1$ GeV. This moment is an integral characteristic of the pion DA and encodes information on the maximum possible weight of the higher-order conformal coefficients. Moreover, it is particularly relevant for phenomenological applications because

$$\langle x^{-1} \rangle_\pi = 3(1 + a_2 + a_4 \ldots) = \frac{3}{\sqrt{2} f_\pi} Q^2 F^{(\mathrm{LO})}_{\gamma^* \gamma \pi^0}(Q^2)\,, \tag{14}$$

where $F^{(\mathrm{LO})}_{\gamma^* \gamma \pi^0}(Q^2)$ is the leading-order (LO) expression of the pion-photon transition form factor, which has been measured in several experiments from a few GeV^2 up to 40 GeV^2 [44–47]. Here the ellipsis represents corrections due to higher eigenfunctions and evolution of the Gegenbauer coefficients a_n to the considered scale Q^2 is assumed (see [6] for more details). Thus, experimental evidence can be used to validate or reject particular pion DAs. For instance, we know (see, e.g., [28]) that all existing data demand $\langle x^{-1} \rangle_\pi > 3$, implying that the π DA has to be broader than φ_{asy} at accessible momentum values.

To obtain the π DA, we employ the following QCD sum rule ($m_\pi = 0$, $f_\pi = 0.137$ GeV)

$$f_\pi^2\, \varphi_\pi(x) e^{-m_\pi^2/M^2} + f_{A_1}^2\, \varphi_{A_1}(x)\, e^{-m_{A_1}^2/M^2} = \int_0^{s_0^{A_1}} \rho_{\mathrm{pert}}\,(s,x)\, e^{-s/M^2} ds + \Phi_\pi(x, M^2)\,, \tag{15}$$

whereas for the $\rho_\parallel$ DA we have

$$f_\rho^2\, \varphi_\rho^\parallel(x) e^{-m_\rho^2/M^2} + f_{\rho'}^2\, \varphi_{\rho'}^\parallel(x)\, e^{-m_{\rho'}^2/M^2} = \int_0^{s_0} \rho_{\mathrm{pert}}\,(s,x)\, e^{-s/M^2} ds + \Phi_\rho(x, M^2) \tag{16}$$

with $m_\rho = 0.775$ GeV and $m_{\rho'} = 1.496$ GeV. The effective A_1-meson state with the decay constant $f_{A_1} = 0.227$ GeV and the mass $m_{A_1} = 1.2712$ GeV comprises the π' and the a_1 mesons and is described by the DA

$\varphi_{A_1}(x)$. The perturbative contribution to the sum rules is expressed via the perturbative spectral density for which we use the corrected expression published as Eq. (1) in the Erratum to [6], viz.,

$$\rho_{\rm pert}^{\rm (NLO)}(x) = \frac{3x\bar{x}}{2\pi^2}\left[1+\frac{\alpha_s(\mu^2)}{4\pi}C_{\rm F}\left(5-\frac{\pi^2}{3}+\ln^2\frac{\bar{x}}{x}\right)\right], \tag{17}$$

where $C_{\rm F} = (N_c^2-1)/2N_c = 4/3$ for $SU(3)_c$.[3] The nonperturbative content of the sum rule is contained in the expression

$$\Phi_{\rho(\pi)}(x,M^2) = \mp\Phi_{\rm 4Q}(x,M^2)+\Phi_{\bar{q}Aq}(x,M^2) +\Phi_{\rm V}(x,M^2)+\Phi_{\rm G}(x,M^2)\,, \tag{18}$$

where M^2 denotes the Borel parameter and s_0 marks in each case the threshold value which separates the lowest resonance state from higher states. To saturate the sum rules for the first $N=10$ moments of $\varphi_{\rho(\pi)}(x)$ [6], we use $s_0 \approx 2.25$ GeV^2. The various contributions, forming $\Phi_{\rho(\pi)}$, pertain to the following terms: (i) $\Phi_{\rm 4Q}$ (four-quark condensate); (ii) $\Phi_{\bar{q}Aq}$ (quark-gluon-antiquark condensate) (iii) $\Phi_{\rm V}$ (vector quark condensate); (iv) $\Phi_{\rm G}$ (gluon condensate). Their explicit expressions can be found in Appendix A of Ref. [48]. The basic assumption here is that higher-order correlations are less important than two-particle correlations (vacuum-dominance hypothesis [59]). This assumption is employed in order to reduce the four-quark condensate to the product of two-quark condensates ignoring corresponding uncertainties. One notes that the four-quark contribution enters the sum rule for $\rho_\parallel$ in (18) with the opposite sign with respect to π. As a result, it reduces the relative weight of this condensate in the sum rule entailing smaller values of the DA moments — in contrast to the pion case. In fact, we found in [8] (see Table 1 there) the following relation: $\langle\xi^{2N}\rangle_\pi \geq \langle\xi^{2N}\rangle_{\rho_\parallel} \geq \langle\xi^{2N}\rangle_{\rm asy}$ with $N=1,2,3,\ldots$.

Similarly to the pion DA, the DA of the longitudinally polarized ρ is defined by the matrix element

$$\langle 0|\bar{d}(z)\gamma_\mu u(0)|\rho(p,\lambda)\big|_{z^2=0} = f_\rho^\parallel p_\mu \int_0^1 dx e^{ix(z\cdot p)} \times\varphi_\rho^\parallel(x,\mu^2)\,, \tag{19}$$

while the definition of the transversal ($\perp$) ρ DA reads

$$\langle 0|\bar{d}(z)\sigma_{\mu\nu}u(0)|\rho(p,\lambda)\big|_{z^2=0} = if_\rho^\perp(\varepsilon_\mu^{(\lambda)}p_\nu-\varepsilon_\nu^{(\lambda)}p_\mu) \times\int_0^1 dx e^{ix(z\cdot p)}\varphi_\rho^\perp(x,\mu^2)\,, \tag{20}$$

where we have again employed the gauge $A^+=0$. The $\rho_\perp$ DA will not be considered in this work.

[3] This expression coincides with the $\mathcal{O}(\alpha_s)$ radiative correction entering the perturbative contribution to the sum rule considered in [17].

To construct $\varphi_\rho^\parallel(x,\mu^2)$, we compute the moments $\langle\xi^N\rangle_{\rho_\parallel}$ up to $N=10$ from the QCD sum rule (16) and determine from them the corresponding conformal coefficients a_n with $N=0,2,\ldots,10$. Because the moments with $N\geq 6$ turn out to have values close to the asymptotic ones, we can safely set the associated conformal coefficients equal to zero and express $\varphi_\rho^\parallel(x,\mu^2)$ in the form of Eq. (9). In addition, we use the Gegenbauer-α expansion, given by Eq. (10), via the parameters (α_-,a_2^α). The accessible regions of these parameters for the longitudinal ρ DA, determined within QCD sum rules with nonlocal condensates, are displayed as shaded blue areas closer to the y axis in Fig. 2. The left panel displays the results in the (a_2,a_4) plane, while the right panel contains the analogous results in the (α_-,a_2^α) plane. We have also depicted in both panels the parameter regions referring to the pion case for $\lambda_q^2=0.4$ GeV^2 (larger green slanted rectangles further to the right) and for $\lambda_q^2=0.45$ GeV^2 (transparent rectangles within dashed boundaries). The graphics in Fig. 2 include the platykurtic regimes of both DAs, determined in our present NLC-based analysis to be outlined later. Those areas referring to $\rho_\parallel$ have red color and are located closer to the ordinate (left panel) and further to the top (right panel). The analogous areas for the pion appear in light green color and are adjacent to the previous ones. In addition, we incorporate several other π and $\rho_\parallel$ DAs with individual designations explained in the figure caption for the readers's convenience. The uncertainties of the presented pion and rho-meson DAs, obtained with our NLC QCD SR approach, include only those stemming from the SRs themselves and are related to the variation of the Borel parameter within the stability window of the SRs [6]. Experimental uncertainties in the input physical parameters have little influence on the results and have been ignored.

The values of all parameters of the displayed models are listed in Table I at the reference scale $\mu^2=4$ GeV^2. This scale is employed in lattice calculations because it naturally arises by the matching of the bare (lattice) operators at $\mu_0^2=1/a^2$ (a being the lattice spacing) to those in the $\overline{\rm MS}$ scheme in continuum QCD. It is also used in various works based on the DSE approach. In this work, we obtained our own results at the initial scale $\mu^2\gtrsim 1$ GeV^2 and evolved them to this higher scale using ERBL evolution at the next-to-leading order level. The conformal coefficients a_2 and a_4, and the moments $\langle\xi^2\rangle$ and $\langle\xi^4\rangle$ along with the inverse moment $\langle x^{-1}\rangle$ in Table I have for each DA their own original values at $\mu^2=4$ GeV^2. In cases where the original scale was lower, we have evolved these quantities to the scale $\mu^2=4$ GeV^2 using two-loop ERBL evolution.

We have included in the table the AdS/QCD model of the pion DA derived in [43] within holographic QCD. This model reads $\varphi_\pi(x,\mu^2) = (4/\sqrt{3}\pi)\sqrt{x\bar{x}}$ and approaches at $Q^2\to\infty$ the asymptotic DA $\varphi_\pi^{\rm asy}(x)=6x\bar{x}$, while it has a very different x behavior at finite Q^2 [43, 50]. The conformal coefficients of this DA have been computed in the arXiv version of [20] at the initial

TABLE I: Various parameters entering the DA Gegenbauer representations in (3) and (10) in the $\overline{\rm MS}$ scheme. The kurtosis β_2, the second moment $\langle\xi^2\rangle$, the fourth moment $\langle\xi^4\rangle$, and the inverse moment $\langle x^{-1}\rangle$ of the π and the $\rho_\parallel$ DAs are also shown. Always the original functional forms of the DAs have been used with the same designations as in Fig. 2. The reference scale for all entries is $\mu^2 = 4$ GeV^2 either by construction or after NLO evolution. Only the central values of the normalization coefficients N_α are displayed. Note that we ignore here and in the figures the numerically negligible effects on the asymptotic DA induced by NLO evolution [32].

Model DA	a_2	a_4	N_α	α_-	a_2^α	β_2	$\langle\xi^2\rangle$	$\langle\xi^4\rangle$	$\langle x^{-1}\rangle$
asy ◆	0	0	6	1	0	2.14	0.2	0.086	3
$\rho_\parallel$ [18] ♦	0.056	-0.055	16.83	1.63	0.137	1.93	0.22	0.093	3.0
$\rho_\parallel$ [8] ★	0.032(46)	-0.038(81)	13.6	$1.50^{+0.71}_{-1.50}$	$0.11^{+0.08}_{-1.14}$	2.0(3)	0.211(16)	0.088(7)	3.0(1)
$\rho_\parallel^{\rm pk}$ (here) ✪	0.017(24)	$-0.021(11)$	10.0	$1.312^{+0.19}_{-0.171}$	$0.071^{+0.016}_{-0.015}$	2.06(4)	0.206(8)	0.087(6)	3.0(8)
$\rho_\parallel$ [40] ●	-0.009	-0.023	11.81	1.41	0.063	2.09	0.197	0.081	2.92
$\rho_\parallel$ [39] ▼	0.012	-0.007	7.18	1.11	0.034	2.11	0.204	0.088	2.98
$\rho_\parallel$ [41] ■	0.10	0	6	1	0.10	1.98	0.234	0.109	3.30
$\rho_\parallel$ [10] ◊	0.092	0.031	3.37	0.66	0	2.05	0.232	0.110	3.5
$\rho_\parallel$ [42] □	0.057	0.002	5.76	0.975	0.052	2.05	0.220	0.099	3.2
$\pi_{\rm BMS}$ [6] ✖	$0.149^{+0.052}_{-0.043}$	$-0.096^{+0.063}_{-0.058}$	20.49	$1.76^{+0.30}_{-0.45}$	$0.217^{+0.048}_{-0.066}$	$1.74^{+0.16}_{-0.14}$	$0.248^{+0.016}_{-0.015}$	$0.108^{+0.05}_{-0.03}$	$3.16^{+0.09}_{-0.09}$
$\pi_{\rm pk}$ [5] ✜	$0.057^{+0.024}_{-0.019}$	$-0.013^{+0.022}_{-0.019}$	7.78	$1.16^{+0.24}_{-0.26}$	$0.086^{+0.019}_{-0.026}$	$2.02^{+0.02}_{-0.03}$	$0.220^{+0.009}_{-0.006}$	$0.098^{+0.008}_{-0.005}$	$3.13^{+0.14}_{-0.10}$
$\pi_{\rm DSE-DB}$ [9] ▲	0.149	0.076	1.81	0.31	-0.12	2.0	0.251	0.128	4.6
$\pi_{\rm DSE-RL}$ [9] ▽	0.233	0.112	1.74	0.29	0.0029	1.9	0.280	0.151	5.5
$\pi_{\rm AdS/QCD}$ [43] △	0.107	0.038	2.55	0.50	0	2.03	0.237	0.114	4.0 [a]
$\pi_{\rm CZ}$ [1]	0.42	0	6.0	1.0	0.42	1.54	0.343	0.181	4.25
$\pi_{\rm lat}$ [49]	0.1364(154)(145)	–	–	–	–	–	0.2361(41)(39)	–	–

[a] This value was obtained using only the first three terms of the conformal expansion in Eq. (3) and is therefore not a precise estimate.

scale $\mu^2 \approx 1$ GeV^2 to obtain $\langle\xi^2\rangle^{\rm AdS/QCD} = 0.250$ and $\langle\xi^4\rangle^{\rm AdS/QCD} = 0.125$ from which the first two conformal coefficients $a_2^{\rm AdS/QCD} = 7/48$ and $a_4^{\rm AdS/QCD} = 11/192$ were determined. Using NLO scaling relations, these coefficients have been evolved to the reference scale $\mu^2 = 4$ GeV^2 and are given in Table I. The value of the second moment was later computed in [50] for $\mu_0 = 1$ GeV and $\Lambda_{\rm QCD} = 0.225$ GeV using LO evolution and found to be almost the same, notably, $\langle\xi^2\rangle^{\rm AdS/QCD}_{\mu^2=4\ {\rm GeV}^2} = 0.24$. Note that a broad pion DA $\sim \sqrt{x\bar{x}}$ was considered before in [13, 16] using QCD sum rules with NLCs. An even broader DA was discussed earlier in [51], giving $\varphi_\pi(x) \sim (x\bar{x})^{[0.1-0.2]}$. To complete this discussion, we mention that the coefficient a_2 (and other parameters) for the pion DA proposed by Chernyak and Zhitnitsky [1] has been included in Table I using NLO evolution to the scale $\mu^2 = 4$ GeV^2, but we have not displayed it in Fig. 2 because its value is outside the range of the graphs.

The most important observations from Fig. 2 are the following: (i) There is no overlap of the (a_2, a_4), or, equivalently, (α_-, a_2^α), regions for the pion and the $\rho_\parallel$ meson computed with NLC sum rules in [6] and [8]. (ii) While the platykurtic regime for the $\rho_\parallel$ DA is entirely enclosed by the region determined with $\lambda_q^2 = 0.4$ GeV^2, the platykurtic regime for the pion DA appears as an exclave. This is, because in order to obtain a platykurtic pion DA one has to use the slightly larger value $\lambda_q^2 = 0.45$ GeV^2. (iii) The DSE-based DAs for the pion and the $\rho_\parallel$ meson are in both panels far away from our NLC estimates. But keep in mind that the locations of the DSE DAs in the (a_2, a_4) plane are only indicative because, as we have already mentioned, their parametrization by means of Eq. (9) is a very crude approximation. (iv) We observe in the (a_2, a_4) plane an intriguing alignment of the unimodal DSE-based DAs (π and $\rho_\parallel$) along an upward pointing "diagonal" and another branch of bimodal NLC-based DAs steered downwards along $a_2 + a_4 \approx$ const. This second "orbit" of DAs roughly follows the values of $\langle x^{-1}\rangle_\pi/3 - 1$ evolved to the scale 4 GeV^2 [6]. Crucially, there is a small region where both branches overlap allowing the combination of endpoint suppression with unimodality — the chimera regime of our interest. (v) On the other hand, all DAs, blended together according to Eq. (26), lie on the straight line with $a_2 \cong 0.15$ and stray away from the NLC (a_2, a_4) region with decreasing values of the mixing parameter a. Ultimately, i.e., for $Q^2 \to \infty$, all DAs with the correct x asymptotics will evolve either along the upper "diagonal" (if they are unimodal) or along the lower one (if they are bimodal) toward the asymptotic DA (◆)

with $\gamma_0 = 0$, as predicted by perturbative QCD. Issues (iv) and (v) will be addressed later in full detail.

V. MESON DAs AS PATTERNS OF SYNCHRONIZATION

The meson DA at a fixed scale μ^2 is a distribution of x values in the interval $[0,1]$. While a unimodal DA profile may seem more "natural" in appearance for the ground state of the pion, the interpretation of a bimodal structure causes discomfort and gives rise to debates. So there is a desire for an explanation and rationalization of this issue.

Recently, it was argued by one of us [4] that in order to better understand the patterns of the pion and other meson DAs it is useful to develop some ideas which are drawn from the subject of synchronization of nonlinear oscillators in the theory of complex systems — natural and engineered (see [52, 53] for reviews). The nub of the idea, as Stefanis put it in Ref. [4], is to represent the x values, accessible to the meson DAs in the interval $[0,1]$, in terms of the phases of a large number ($N \to \infty$) of interacting oscillators. The dynamics of this kind of systems is describable in terms of the Kuramoto model [54] and its descendants, albeit its specifics is not relevant for the present analysis. What is more important is that the synchronization of the oscillator phases, alias the longitudinal momentum fractions carried by the valence quark vs. that of the antiquark, gives rise to the formation of particular patterns of the x distribution. These patterns emerge from the "organization" of the phase spectrum (i.e, the x distribution) and reflect the specific approach used to describe the partonic interactions in the pion bound state described by the DA. In other words, each particular DA profile is latent in the underlying theoretical method and pertains to a patterned arrangement of synchronized coupled oscillators in the Kuramoto context.

These methods can be QCD sum rules with nonlocal condensates, as employed in this work and in [6, 8] (see also [22, 28]), local condensates [1], lightcone sum rules (LCSR)s [23, 55], instanton models [40], approaches based on Dyson–Schwinger-equations [9, 10] (reviewed in [56]), light-front models, e.g., [39, 57], holographic QCD [43, 50] — see [58] for a recent review, etc. Examples of π and $\rho_\parallel$ DA profiles are depicted in Fig. 1. Thus, the Sync concept provides a universal canvas to study the characteristics of very different meson DAs without taking recourse to a specific calculational scheme. In particular, it puts a theoretical basis beneath the interpretation of the bimodality of meson DAs, as we will show next.

Indeed, it was pointed out in [4] that at scales of the order of $\mu \sim 1-2$ GeV, nonlocal condensates, which are used to parameterize the vacuum nonlocality in terms of a nonvanishing quark virtuality λ_q^2 cause the distribution over x to flock into two clusters, giving rise — within a broad range of uncertainties in the midregion of x — to bimodal DAs for the pion [6] and the $\rho_\parallel$ meson [8]. The corresponding families of DAs are shown in the form of the larger shaded bands in Fig. 1. The upper panel refers to the π and the lower one to the $\rho_\parallel$ meson, both at the scale $\mu^2 = 4$ GeV^2 after NLO evolution from the initial scale $\mu_0^2 \sim 1$ GeV^2.

The bimodality strength of the BMS-type of DAs is controlled by the nonlocality parameter λ_q^2, which endows vacuum fluctuations with a characteristic correlation length $\sim 1/\lambda_q$. Lower values of λ_q^2 tend to increase the bimodality character of the DA and reduce the value of $\varphi_\pi(x=1/2)$, while larger values enhance the midregion of x driving $\varphi_\pi(x)$ closer to a unimodal distributional shape. This behavior is deeply rooted in the combined effect of the perturbative part and the power-behaved terms in the QCD sum rule for the moments $\langle \xi^N \rangle$ considered in [6] and in [8]. For $\lambda_q^2 = 0$, one recovers the QCD sum rules of Chernyak-Zhitnitsky in Ref. [1] with an infinite correlation length of the vacuum fluctuations. The numerically most important term is the scalar-condensate contribution [13], encountered in (18),[4]

$$\begin{aligned}\Phi_S\left(x;M^2;\Delta\right) = \frac{A_S}{M^4}\frac{18}{\bar{\Delta}\Delta^2}\,\{\theta\left(\bar{x}>\Delta>x\right)\bar{x}\,[x \\ + (\Delta - x)\ln\left(\bar{x}\right)] + (\bar{x}\to x) + \theta(1>\Delta) \\ \times\,\theta\left(\Delta>x>\bar{\Delta}\right)\left[\bar{\Delta} + (\Delta - 2\bar{x}x)\right. \\ \left.\times\ln(\Delta)\right]\}\,, \end{aligned} \tag{21}$$

where $A_S = (8\pi\alpha_s/81)\langle\bar{q}q\rangle^2$, with the four-quark contribution being given by $\alpha_s\langle\bar{q}q\rangle^2 = 1.83\times10^{-4}$ GeV^6 and $\langle\alpha_s GG\rangle/12\pi = 0.0012$ GeV^4 [59]. Here, $\Delta = \lambda_q^2/2M^2$, $\bar{\Delta} \equiv 1-\Delta$, and $M^2 \approx 1$ GeV^2 is the Borel parameter $M^2 \in [M^2_{\rm min}, M^2_{\rm max}]$. The sum rule should not be sensitive to the choice of this parameter. The procedure for minimizing the dependence on M^2 has been described in [48] and is applied here.

Larger values of Δ shift the balance in the sum rule in favor of the perturbative contribution which has a single mode at $x = 1/2$, thus entailing a reduction of the two peaks at $x_0 = \Delta$ and $x_0 = \bar{\Delta}$ until they ultimately collapse into a single more rounded peak at the center. But despite this shift towards the central region of x, the tails of the BMS DAs remain suppressed within only a small range of theoretical uncertainties, as one also observes from Fig. 1. Moreover, it was shown in [48] that the endpoint behavior of the pion DA can be related to the "decay rate" of the correlation length of the scalar condensate. It is worth noting in this context that in the local version of the condensate model, i.e., for $\lambda_q^2 = 0$, all nonperturbative contributions are concentrated just at the endpoints because $\Phi_{\rm 4Q}^{\rm local}(x) = 9\left[\delta(x) + \delta(\bar{x})\right]/(M^2)^2$.

Viewed from the Kuramoto prism, the two peaks of the BMS DAs correspond to two distinct groups of rather

[4] The expression for the scalar quark-condensate contribution in Eq. (21) pertains to a Gaussian model for the quark condensate.

strongly synchronized oscillators with characteristic "frequencies" located in the lower and upper quartiles of the x distribution, respectively. On the other hand, the tails correspond to tiny cohorts of oscillators with natural "frequencies" close to the rare values $x = 0$ and $x = 1$ with almost nil phase-locking, while a partly synchronized arrangement of oscillators with values around $x = 1/2$ connects the two clusters across the dip in the central region.

Consider now the implementation of DCSB to meson DAs. It was stated in [4] that the DCSB and the concomitant mass generation of quarks and gluons within the DSE-based framework [9, 10] tend to enhance, both the central region of x values but also the tails of the meson DAs down to the kinematic endpoints $x = 0, 1$, leading to a homogenization of the x values of the valence $\bar{q}q$ pair and to broad unimodal DAs for all considered mesons [9, 10, 60, 61]. These DAs have downward concave profiles in the whole interval $x \in [0, 1]$. There are two variants of pion DAs derived from the DSE-based approach [9]. They were computed via a large number of moments $\langle (x - \bar{x})^N \rangle$ ($N = 50$) and were then expressed by means of Eq. (12) using two different DSE truncations at the scale $\mu^2 = 4$ GeV^2. The associated values of the parameters $(N_\alpha, \alpha_-, a_2^\alpha)$ and other relevant metrics are provided in Table I.

One π DA, dubbed DSE-RL, was obtained using the rainbow-ladder (RL) approximation of the Bethe–Salpeter kernel in the DSEs, while the other, termed DSE-DB, was derived with a DCSB-improved kernel (abbreviated by DB), which includes nonperturbative DCSB-generated effects that were not taken into account in the RL truncated version. Both DAs are much broader relative to $\varphi_\pi^{\rm asy}$, with the DSE-RL DA being flatter and broader than the DSE-DB DA. The profiles of these DAs are given in the upper panel of Fig. 1: DSE-RL — dashed-dotted line; DSE-DB — dashed line. Also the $\rho_\parallel$ DA obtained with the DSE computational scheme [10], is a relatively broad everywhere downward concave curve (though less pronounced than both pion DSE DAs), as one can see from the lower panel of Fig. 1 (lower dashed line). The broadening of the DSE DAs is a direct consequence of the nonperturbative DCSB interactions which give rise to the dressed quark's selfenergy — see [56] for a detailed review of the method and further explanations. Also note that the DSE DAs cross the NLC-based ones twice on each side of the mean (Fig. 1). Thus, these DAs show a pattern of higher-lower-higher on each side, related to their heavier tails. This behavior can be quantified by employing the kurtosis statistic, defined by

$$\beta_2[\varphi] = \frac{E(x - \mu[\varphi])^4}{(E(x - \mu[\varphi])^2)^2} = \frac{\mu_4[\varphi]}{\sigma^4[\varphi]} = \frac{\langle \xi^4 \rangle_\pi}{\left(\langle \xi^2 \rangle_\pi\right)^2}\,, \qquad (22)$$

where

$$\sigma^2[\varphi] = \int_0^1 dx (x - \mu[\varphi])^2 \varphi(x) = \frac{1}{4}\langle \xi^2 \rangle_\pi \qquad (23)$$

is the variance of the distribution $\varphi(x)$. Together with the skewness (vanishing here but being relevant for mesons composed of light and heavy quarks like the kaon)

$$\gamma_1[\varphi] = \frac{E(x - \mu[\varphi])^3}{\sigma^3[\varphi]}\,, \qquad (24)$$

it describes the central tendency, variability, and shape of a distribution. In particular the kurtosis serves to measure the peakedness in the central region of a distribution against the flatness of its tails. As one sees from Table I, the unimodal, downward concave DSE-based DAs can be ordered as follows: $\beta_2^{\rho_\parallel} > \beta_2^{\pi_{\rm DB}} > \beta_2^{\pi_{\rm RL}}$. This result confirms a similar qualitative statement in [10].

Such broad DA morphologies describe a loosely synchronized assortment of oscillators spread over the entire range of their native "frequencies" in $x \in [0, 1]$. The enhancement of the generic midregion, which corresponds — from a physical perspective — to "egalitarian" partonic configurations in the pion in which the valence quark and the valence antiquark carry comparable fractions of longitudinal momentum, may be welcome. But at the same time DSE DAs also overestimate the weight of "aristocratic" configurations with low probability occurrence in which a single valence parton takes the lion's share of the momentum with $x \to 1$ or $\bar{x} \to 1$ to go far-off shell. Because these are more specific and rare configurations of the dispersion of the valence parton's longitudinal momentum far away from the typical values around the mean $\mu = 1/2$, tail enhancement is at odds with our understanding of the QCD description of the pion bound state based on off-shell gluon exchanges (see [62, 63] and [50] for explanations) and, as we have seen, leads to more variation in the oscillator "frequencies", thus entailing less synchronization. Note that the broader and flatter a unimodal downward concave x distribution is, the closer to random the oscillator phases will be.

Comparison in earlier works, e.g., [5, 7, 28], of predictions for the pion-photon transition form factor obtained within the LCSR framework with all existing data, indicates that strict QCD scaling behavior at high Q^2 is very sensitive to the endpoint-behavior of the pion DA. This behavior is intimately related to the inverse moment $\langle x^{-1} \rangle_\pi$. Recalling Eq. (14), this implies that the conformal coefficients have to balance each other in such a way so that the excess over $\langle x^{-1} \rangle_\pi^{\rm asy} = 3$ is not too large. Otherwise, the form factor would overshoot the data. And in fact, using the DSE DAs as nonperturbative input in a LCSR-framework, we have shown [5] that the predictions obtained herewith exceed the asymptotic limit even at the highest momenta around 40 GeV^2 probed in current experiments [46, 47]. This is also obvious from Table I. The inverse moment

$$\langle x^{-1} \rangle_\pi = \frac{1 + 2\alpha_-}{\alpha_-}\left(1 + a_2^\alpha + \ldots\right)\,, \qquad (25)$$

obtained with both pion DSE DAs, has very large values to be compatible with the data. We mention in this context that a recent analysis [64] of the meson structure in

lightfront holographic QCD, which employs a broad unimodal π DA, finds predictions for the pion-photon transition form factor that are in quite poor agreement with all experimental data (see Fig. 18 there). But notice that a subsequent DSE-based computation [66] of the TFF, in which the role of the inverse moment is not so crucial, finds good agreement with the CELLO, CLEO, and Belle data in the entire domain of spacelike momenta.

In the Sync analogy, the NLC within our approach causes a generic clustering of the DA into two clusters liaised with massive endpoint suppression — within the range of intrinsic theoretical uncertainties — and only a moderate reduction of the DA in the central region, which is controlled by the strength of the nonlocality parameter as discussed above in connection with Eq. (21). Thus, configurations with a highly asymmetric dispersion of the valence parton's longitudinal momentum are suppressed. It is highly unlikely that the pion can remain intact and rebound as a whole for such partonic configurations. In the Sync analogy they would play the role of very idiosyncratic oscillators incapable to synchronize, being either too slow (with "frequency" values close to 0) or too fast with "frequencies" tending to unity. In this sense, the NLC acts like a negative feedback opposing the excessive DCSB-induced enhancement in the endpoint regions by turning off the corresponding oscillators. A figurative explanation of these issues is provided in Fig. 3 in which the two main antithetic effects in the x behavior of the valence quark in the pion DA are illustrated. This is how Stefanis envisioned and mapped out the Sync properties of the BMS-like and DSE-like pion DAs in [4]. So there are, it seems, two very distinct DA patterns with telltale signatures that include, but are not limited to, the pion case: One is related to NLCs, which encode particle correlations in the range $1/\lambda_q \sim 0.3$ fermi, while the other implements DCSB which causes the dynamical generation of quark masses and entails dressing of the quark propagator describing the confined quark in the pion. Both effects are manifestations of confinement and neither exists in isolation — see [67] for a recent review of strong-interaction dynamics. Unfortunately, they cannot be described simultaneously within a single analytic approach at present. Thus, for the time being, there are two physical paradigms with their own computational techniques, each applying only within its own sphere of acceptance and validity.

VI. SYNTHETIC MESON DAs

There are basically two options: (i) Either the x distribution of the pion DA is described by a single DA over the whole range of values in the interval $x \in [0, 1]$, or (ii) the "true" pion DA is rather a mixture of two different DAs, one better applicable to the central region and the other controlling the tails. The first option was discussed above and at length in the literature. Following the second scenario, Stefanis proposed in [4] a synthetic DA of

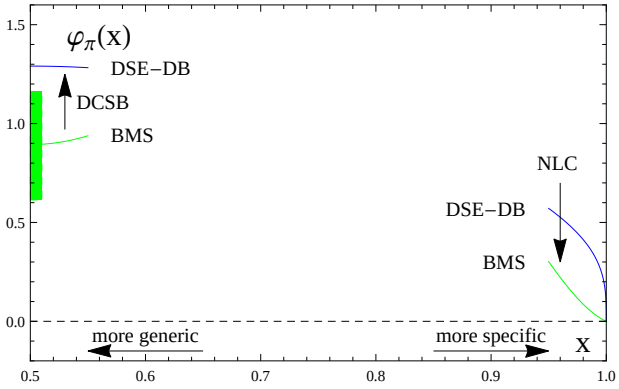


FIG. 3: (color online). Illustrating the key antithetic effects in the pion distribution amplitude in the interval $[0.5, 1]$ (mirror graph in the interval $[0, 0.5]$ not shown). The lower (green) line denotes the BMS DA, with the range of such DAs being indicated by the green vertical strip (cf. green shaded band in the upper panel of Fig. 1). The upper (blue) line marks the DSE-DB DA in the central x region. The unimodal DSE-DB DA shows enhancement of the tails and the midregion around $x = 0.5$, while the BMS π DAs are characterized by suppression of the endpoint region $x = 1$. The corresponding main trends are indicated by vertical arrows: DCSB — enhancement; NLC — suppression.

the form

$$\varphi_\pi^{\rm true}(x, a) = a\varphi_\pi^{\rm BMS}(x) + (1 - a)\varphi_\pi^{\rm DSE}(x) \ , \qquad (26)$$

where a is a mixing parameter with values within the interval $[0, 1]$. Mixtures of the form of Eq. (26) are quite common in statistics when a single distribution, like the Gaussian distribution function, the Poisson distribution, etc., has to be combined with a distribution with a different type of mathematical behavior in the tails, e.g., the generalized Pareto distribution. In fact, hybrid-like DAs have been constructed and profoundly studied by Bergmann and Stefanis long ago for the nucleon [68–70] and also for the $\Delta^+(1232)$ resonance [71] (termed "heterotic" DAs), although they were motivated by other concerns. A comprehensive and detailed review of such baryon DAs has been given in [3]. In the present case, the coexistence of distinct domains of oscillators, some coherent and phase-locked (BMS peaks), and others which describe unsynchronized oscillators (heavy tails of the DSE DA), would give rise to a so-called chimera state [72, 73].

It was argued in [4] that for values of the mixing coefficient a close to 1, the synthetic DA would still belong to the family of pion BMS DAs shown in terms of the wide shaded band in Fig. 1. More generally, the synthesized DA is supposed to encapsulate both manifestations of QCD confinement, reflecting the perpetual balance which arises from the appropriate combination of the two basic effects, one associated with NLC formation, via QCD sum rules (BMS-DA [6]), the other being the result of DCSB, expressed in terms of a DA computed within the DSE-based approach [9]. A proper combination has to

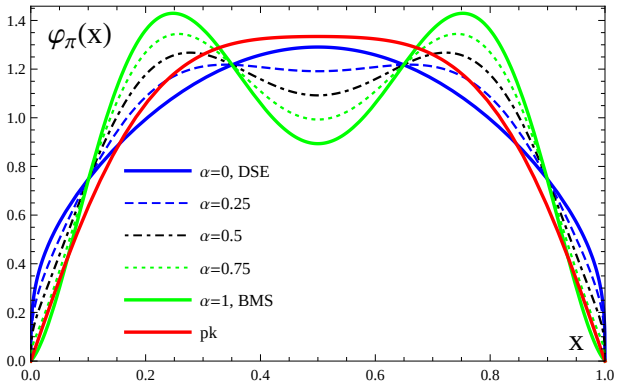


FIG. 4: (color online). Synthetic pion DAs obtained with Eq. (26) at the scale $\mu^2 = 4$ GeV^2 for various values of the mixing parameter $a \in [0, 1]$. The shorttailed platykurtic (pk) DA is shown by the upper red solid line for comparison; it does not belong to this class of DAs (see text).

balance the enhancement impact of DCSB against the suppression due to NLC, as exposed in Fig. 3.

Under ERBL evolution the synthetic DA would develop at $Q^2 \to \infty$ to the asymptotic DA which represents the most synchronized configuration of the valence $\bar{q}q$ pair within the pion being still a bound state [4] after all quark-gluon interactions have died out. This is also evident from Table I from which we see that the asymptotic DA has the largest kurtosis, i.e., $\varphi_{\rm asy}$ is the most leptokurtic meson DA. In this paper, we work out Eq. (26) in more certain terms and exploit the whole range of possible values of a. From the synchronization point of view, a synthetic DA represents an attempt of combining ensembles of synchronized and unsynchronized (but otherwise identical) oscillators in order to enhance or suppress particular frequency values amounting to a chimera state. The question is whether the simple one-parametric design of Eq. (26) is indeed capable of providing the desired properties addressed above in the adjunct discussion of Fig. 3.

Figure 4 shows various samples of synthesized DAs obtained with different values of the mixing parameter between 0 and 1. As one clearly sees from these plots, when a is larger than, say, 0.75, the main characteristics of the BMS DAs persist. This is also obvious from the location of this DA, denoted by the symbol (③), in the plane (a_2, a_4) in the left panel of Fig. 2. However, for small a values close to 0.25 and below, the obtained DA profiles show no endpoint suppression, as desired, but exhibit instead tail enhancement, inherited to them by the DSE DA, while the profile is still bimodal, see ① ($a = 0.25$) and ② ($a = 0.5$) in the same figure. This means that the bimodality of the DA prevails from large down to quite small values of the mixing parameter while at the same time for these small values of a the tails of the DA get strongly enhanced. Hence, Eq. (26) cannot supply a pion DA which combines unimodality in the central region with suppression of the tails, despite the fact that it generates DAs with the same value of a_2, see, Fig. 2, left panel. Nor can this be realized via ERBL evolution.[5] In order to embody endpoint suppression of the pion DA, one has to build it in right from the start, resorting to QCD sum rules with NLCs and looking for DAs which would mimic the characteristics of the DSE DAs in the central region, while preserving suppression of the tails in compliance with Fig. 3. To achieve this goal we have to keep in mind that if mass is moved from the shoulders to the center of a distribution, then one has to compensate the accompanying movement of mass to the tails, leaving the variance almost unchanged but increasing the kurtosis.

The existence of such a chimera DA for the pion, which binds these diverse aspects of coherence and incoherence into a single DA, was first discussed in [4] and predictions for the pion-photon transition form factor $Q^2 F^{\gamma^*\gamma\pi^0}(Q^2)$ were presented which are fully compliant with all experimental data compatible with QCD scaling. The overall quality of these predictions resembles that of the BMS-type DAs [4, 5]. This can be traced back to the fact that they both lead to an inverse moment with just the appropriate size in order to agree with the $Q^2 F^{\gamma^*\gamma\pi^0}(Q^2)$ data. In fact, a brand-new simultaneous fit to the CLEO [45] and Belle [47] data in [65] favors a profile of the pion DA which is very close to the platykurtic one (see Fig. 1 and Table I). On the other hand, DAs with downward concave shapes in the entire interval $x \in [0, 1]$, will tend to overestimate most data of the Belle Collaboration [47], the reason being that they give rise to large inverse-moment values (Table I) and [4, 5] (see also [64]). [The opposite behavior was found in [66], as already mentioned.]

In this work, we determine a whole domain of such chimera π DAs employing our NLC technology and allowing for a slightly larger value of the quark virtuality, viz., $\lambda_q^2 = 0.45$ GeV^2. The core area of these DAs is illustrated in the upper panel of Fig. 1 in the form of a narrow strip in red color. The corresponding parameters and the range of theoretical uncertainties for both used Gegenbauer parametrizations are given at the reference scale $\mu^2 = 4$ GeV^2 in Table I. This table also includes the brand-new lattice estimates for the second moment $\langle \xi^2 \rangle$ from [49] at the same scale using the $\overline{\rm MS}$ scheme.

Note that this a_2 value was not calculated from the second moment $\langle \xi^2 \rangle$ via Eq. (7) at finite lattice spacing, taking subsequently the continuum limit. Instead, the value of a_2 was calculated directly on the lattice and was then extrapolated to the continuum limit via $\langle \xi^2 \rangle^{\overline{\rm MS}}_{a\neq 0} \Rightarrow a_2^{\overline{\rm MS}}|_{a\neq 0} \Rightarrow a_2^{\overline{\rm MS}}|_{a=0}$. This implies that Eq. (7)

[5] Strictly speaking, evolution in NLO gives a logarithmic modification $\sim (\alpha_s/(4\pi))C_{\rm F} \ln^2[(1-x)/x]$ [32] which obviously affects the endpoint behavior of the meson DA — independently of its shape — albeit endpoint-enhanced DAs receive larger NLO corrections [31]. However, given that at scales $\mu \geq 1$ GeV^2 the running coupling is already sufficiently small, this effect can be safely neglected, see [6].

is broken by lattice artifacts. A small variation in the lattice spacing around 6% may result in an increase of a_2 of the order of 25−30% [49]. The final result at $\mu^2 = 4$ GeV^2 reads $a_2^{\overline{\rm MS}}|_{a=0} = 0.1364(154)(145)$, while the reported value of the second moment is $\langle\xi^2\rangle_\pi^{\rm lat} = 0.2361(41)(39)$. The first error is statistical and originates from the chiral expansion, whereas the second one pertains to the uncertainties of the renormalization factors. It agrees within errors with $\langle\xi^2\rangle_\pi^{\rm BMS} = 0.248\{^{0.264}_{0.233}$ [20] and also with $\langle\xi^2\rangle_\pi^{\rm pk} = 0.220\{^{0.229}_{0.213}$ (see Table I). In contrast, while the lattice estimate $a_2^{\rm lat}$ agrees with the BMS coefficient $a_2^{\rm BMS}$, determined in the year 2001 [6] (see Table I), it turns out to be larger than $a_2^{\rm pk}$. But one should be cautious. Extracting a_2 via $\langle\xi^2\rangle_{a\neq0}^{\overline{\rm MS}} \Rightarrow \langle\xi^2\rangle_{a=0}^{\overline{\rm MS}} \Rightarrow a_2^{\overline{\rm MS}}|_{a=0}$, one would obtain $a_2^{\rm lat} = 0.105$, which is indeed compatible with the range of the platykurtic a_2 values. Thus, one cannot exclude the influence of significant discretization effects that would require simulations at smaller lattice spacings of the order of $a \sim 0.04$ fm [49].

Be that as it may, one should recall that the second moment $\langle\xi^2\rangle_\pi$ is related to the variance of the DA given by Eq. (23). This statistic is not sufficient to draw any conclusions about the shape of the distribution in the central region. Indeed, as one observes from Table I, the unimodal DSE-DB pion DA yields a conformal coefficient $a_2^{\rm DSE-DB} = 0.149$ which fully agrees with the new lattice result but also with $a_2^{\rm BMS}$. We note that this is valid for the second moment as well, which has the value $\langle\xi^2\rangle_\pi^{\rm DSE-DB} = 0.250$, (cf. (7)) and thus almost coincides with the second moment of the pion BMS DA given above, being also close to $\langle\xi^2\rangle_\pi^{\rm pk}$. On the other hand, the fourth moment $\langle\xi^4\rangle$ and the conformal coefficient a_4 of the DSE and the BMS (pk) DAs are different in value and sign, respectively — see Table I. What is far more significant is the fact that, as it is evident from the left panel of Fig. 2, *all* DAs lying on the straight vertical line at $a_2 \cong 0.15$ agree equally well with the new lattice estimate for a_2. This makes it apparent that a single lattice constraint cannot fix the profile of the pion DA uniquely, however precise it may be.

The chimera DAs have shorttailed platykurtic profiles and overlap with the DSE-DB DA in the midregion of x but descend at the endpoints at low angle to zero, similar to a typical BMS DA. As one observes from Fig. 2 (both panels), there is an imbrication of the platykurtic regimes (small rectangles in light-green color) with the domains of the bimodal pion DAs obtained with NLC sum rules for the quark virtuality $\lambda_q^2 = 0.45$ GeV^2 (transparent rectangles bounded by a dashed line). For this value the conformal coefficients for $\varphi_\pi^{\rm BMS}(x)$ at $\mu^2 = 4$ GeV^2 read $a_2 = 0.12$ and $a_4 = -0.06$ while the inverse moment is $\langle x^{-1}\rangle_\pi^{{\rm BMS}(\lambda_q^2=0.45\ {\rm GeV}^2)} = 3.18$, a value which agrees well with $\langle x^{-1}\rangle_\pi^{\rm pk} = 3.13$ in Table I. The prediction for $Q^2F^{\gamma^*\gamma\pi^0}(Q^2)$ obtained with the shorttailed platykurtic π DA appears in line with all data of the Belle [47] and the BaBar Collaboration [46] compatible with QCD scaling [4, 5]. These unique features of the pk pion DA look indeed very attractive. But is it more than mere coincidence or can it provide a general mode of accessing meson DAs and offer a deeper perspective on meson DAs in general?

To this end, we turn our attention to the ρ meson case and attempt to determine a platykurtic regime for the $\rho_\parallel$ DA using as a selector the behavior illustrated in Fig. 3. Evaluating the sum rule in Eq. (16), we compute the reliability range of the conformal coefficients up to the order $N = 10$ by first determining the central moments $\langle\xi^N\rangle_{\rho_\parallel}$ of the same order. Their values at the initial scale $\mu^2 \gtrsim 1$ GeV^2 can be found in [8]. Also the corresponding values of the $\rho'_\parallel$ meson are given there together with the conformal coefficients. We will not repeat these details here. We concentrate instead on our primary goal to extract a platykurtic domain of these parameters. It turns out that this is possible even for the somewhat smaller value of the quark virtuality $\lambda_q^2 = 0.4$ GeV^2 used originally for the extraction of the pion DA in [6]. The extracted domains are shown in Fig. 2 in the form of the red slanted rectangles surrounded by the larger blue bands of coefficient values computed with the NLC sum rules. The left panel displays the results for the first two conformal coefficients a_2 and a_4, whereas the right panel provides the areas of the coefficients α_- and a_2^α. In both graphics the platykurtic model for the $\rho_\parallel$ DA is denoted by the symbol ✪. The values of all these parameters, accompanied by their intrinsic errors, are compiled in Table I, while the platykurtic $\rho_\parallel$ DA profiles are displayed in the form of a narrow red strip in the lower panel of Fig. 1. For the sake of direct comparison with the DSE results, all graphics and the values in the table are given at the reference scale $\mu^2 = 4$ GeV^2 after two-loop evolution. One immediately observes from this figure that, similar to the pion case, the platykurtic $\rho_\parallel$ DA has a single rounded central peak bearing endpoint suppression relative to the $\rho_\parallel$ DA obtained within the DSE-based approach [10]. In comparison to the platykurtic DA of the pion, it features a slightly narrower profile with the kurtosis value $\beta_2^{\rho_\parallel^{\rm pk}} > \beta_2^{\pi^{\rm pk}}$. Tangible consequences of the platykurtic $\rho_\parallel$ DA will be studied elsewhere.

VII. CONCLUSIONS

We have performed an intensive study of the pion and the $\rho_\parallel$ DAs within QCD, fortified with the knowledge of synchronization concepts used in the description of complex systems. These concepts provide a unifying rationale of *how* the various DA profiles emerge instead of asking *why* they should have a particular shape, thus avoiding descriptive comparisons of DAs obtained with unrelated theoretical frameworks. Furthermore, guided by these concepts, we have used controlled theory tools to obtain a new kind of chimera DAs for the pion and the $\rho_\parallel$ meson using QCD sum rules with NLCs. These DAs are capable of mingling in situ the best of both worlds —

endpoint suppression via NLC and unimodality due to DCSB, giving rise to shorttailed platykurtic profiles and realizing the scenario illustrated in Fig. 3, while preserving the asymptotic x behavior predicted by perturbative QCD. In the Sync picture, they correspond to a vast number of phase-locked oscillators between the lower and the upper quartile of the x distribution, whereas oscillators with extremely high or low "frequencies", located close to the tails $x = 0, 1$, are in limbo. While the characteristics of these new DAs in the central x region resemble the gross behavior of DSE-based DAs, their suppressed tails are following the same trend as the BMS DAs. In mathematical terms, the BMS-like DAs and the platykurtic ones are very different as regards their profiles (Fig. 1) and Gegenbauer coefficients (Fig. 2 and Table I). But from the NLC point of view, the bimodal BMS π DAs and the bimodal $\rho_{\|}$ DA of [8], which in the Sync analogy correspond to two clusters of synchronized oscillators, are on the same theoretical footing as the unimodal shorttailed platykurtic DAs for these mesons, which unite the phase-locked oscillators in a single group. Moreover, in the pion case they yield coinciding predictions for the pion-photon transition form factor which agree well with all available experimental data compatible with QCD scaling above ~ 9 GeV^2. Given all these results, we don't want to stretch the importance of unimodality too far.

Too broad DAs with downward concave profiles encompassing the tails, as those derived for mesons with the aid of DSEs [9, 10], imply that there is no particular x value standing out because even the remote regions close to the endpoints $x = 0, 1$ have a significant weight almost comparable to that of the central region — especially the DSE-RL pion DA. The extreme case of a flat-top DA, like $\varphi_\pi^{\text{flat-top}}(x) = \Gamma(2(\alpha+1))[\Gamma^2(\alpha+1)]^{-1}(x\bar{x})^\alpha$ with $\alpha = 0.1$ [48], translates into a population of oscillators with a very strong variation of native "frequencies" so that these oscillators can hardly synchronize and as a result phase locking diminishes. Physically, this kind of x distribution comprises extremely asymmetric partonic configurations that can spoil scale locality and thus collinear factorization. On the experimental side, flat-top DAs yield predictions for the scaled pion-photon transition form factor which have a tendency to increase with Q^2 — at least in the domain of currently accessible momentum values in the range 10-40 GeV^2 where one would expect scaling to be visible [28]. The high-Q^2 data of the BaBar Collaboration [46] indicate such a trend, but are not supported by the Belle data [47] in the same region. The next-generation experiments to measure the pion-photon transition form factor with the Belle II detector at the upgraded KEKB accelerator (SuperKEKB) in Japan and more precise data on the electromagnetic pion form factor expected at the Jefferson Laboratory (JLab) after its upgrade will provide extraordinary tools to test our predictions and assertions.

Acknowledgments

We thank Sergey Mikhailov for collaboration on various aspects related to the present work and for useful discussions and comments. A.P. thanks Pengming Zhang for the warm hospitality and support at the Institute of Modern Physics of the Chinese Academy of Sciences, where the final stage of this work was carried out. This work was partially supported by the Heisenberg–Landau Program (Grant 2015), the Russian Foundation for Fundamental Research under Grants No. 14-01-00647 and No. 15-52-04023, the JINR-BelRFFR grant F14D-007, the Major State Basic Research Development Program in China (No. 2015CB856903), and the National Natural Science Foundation of China (Grant No. 11575254 and 11175215).

[1] V. L. Chernyak and A. R. Zhitnitsky, Phys. Rept. **112** (1984) 173.
[2] S. J. Brodsky and G. P. Lepage, Adv. Ser. Direct. High Energy Phys. **5** (1989) 93.
[3] N. G. Stefanis, Eur. Phys. J. direct C **7** (1999) 1, hep-ph/9911375.
[4] N. G. Stefanis, Phys. Lett. B **738** (2014) 483, arXiv:1405.0959.
[5] N. G. Stefanis, S. V. Mikhailov, and A. V. Pimikov, Few Body Syst. **56** (2015) 295, arXiv:1411.0528.
[6] A. P. Bakulev, S. V. Mikhailov, and N. G. Stefanis, Phys. Lett. B **508** (2001) 279, hep-ph/0103119; A. P. Bakulev, S. V. Mikhailov, and N. G. Stefanis, Phys. Lett. B **590** (2004) 309 (Erratum).
[7] A. P. Bakulev, S. V. Mikhailov, and N. G. Stefanis, Phys. Rev. D **73** (2006), 056002, hep-ph/0512119.
[8] A. V. Pimikov, S. V. Mikhailov, and N. G. Stefanis, Few Body Syst. **55** (2014) 401, arXiv:1312.2776.
[9] L. Chang, I. C. Cloet, J. J. Cobos-Martinez, C. D. Roberts, S. M. Schmidt, and P. C. Tandy, Phys. Rev. Lett. **110** (2013) 132001, arXiv:1301.0324.
[10] F. Gao, L. Chang, Y.-X. Liu, C. D. Roberts, and S. M. Schmidt, Phys. Rev. D **90** (2014) 014011, arXiv:1405.0289.
[11] A. V. Efremov and A. V. Radyushkin, Theor. Math. Phys. **42** (1980) 97.
[12] G. P. Lepage and S. J. Brodsky, Phys. Rev. D **22** (1980) 2157.
[13] S. V. Mikhailov and A. V. Radyushkin, JETP Lett. **43** (1986) 712.
[14] S. V. Mikhailov and A. V. Radyushkin, Sov. J. Nucl. Phys. **49** (1989) 494.
[15] A. P. Bakulev and A. V. Radyushkin, Phys. Lett. B **271** (1991) 223.
[16] S. V. Mikhailov and A. V. Radyushkin, Sov. J. Nucl. Phys. **52** (1990) 697.
[17] S. V. Mikhailov and A. V. Radyushkin, Phys. Rev. D **45** (1992) 1754.

[18] A. P. Bakulev and S. V. Mikhailov, Phys. Lett. B **436** (1998) 351, hep-ph/9803298.

[19] A. P. Bakulev, S. V. Mikhailov, and N. G. Stefanis, Annalen Phys. **13** (2004) 629, hep-ph/0410138.

[20] N. G. Stefanis, Nucl. Phys. Proc. Suppl. **181-182** (2008) 199, arXiv:0805.3117.

[21] N. G. Stefanis, A. P. Bakulev, S. V. Mikhailov, and A. V. Pimikov, Phys. Rev. D **87** (2013) 094025, arXiv:1202.1781.

[22] A. P. Bakulev, S. V. Mikhailov, A. V. Pimikov, and N. G. Stefanis, Phys. Rev. D **84** (2011) 034014, arXiv:1105.2753.

[23] S. S. Agaev, V. M. Braun, N. Offen, and F. A. Porkert, Phys. Rev. D **83** (2011) 054020, arXiv:1012.4671.

[24] A. P. Bakulev, S. V. Mikhailov, and N. G. Stefanis, Phys. Rev. D **67** (2003) 074012, hep-ph/0212250.

[25] A. P. Bakulev, S. V. Mikhailov, and N. G. Stefanis, Phys. Lett. B **578** (2004) 91, hep-ph/0303039.

[26] A. P. Bakulev, N. G. Stefanis, and O. V. Teryaev, Phys. Rev. D **76** (2007) 074032, arXiv:0706.4222.

[27] S. V. Mikhailov and N. G. Stefanis, Nucl. Phys. B **821** (2009) 291, arXiv:0905.4004.

[28] A. P. Bakulev, S. V. Mikhailov, A. V. Pimikov, and N. G. Stefanis, Phys. Rev. D **86** (2012) 031501, arXiv:1205.3770.

[29] S. V. Mikhailov, A. V. Pimikov, and N. G. Stefanis, Few Body Syst. **55** (2014) 367, arXiv:1401.4303.

[30] S. V. Mikhailov and A. V. Radyushkin, Nucl. Phys. B **273** (1986) 297.

[31] D. Müller, Phys. Rev. D **49** (1994) 2525.

[32] D. Müller, Phys. Rev. D **51** (1995) 3855, hep-ph/9411338.

[33] E. G. Floratos, D. A. Ross, and C. T. Sachrajda, Nucl. Phys. B **129** (1977) 66.

[34] A. Gonzalez-Arroyo, C. Lopez, and F. J. Yndurain, Nucl. Phys. B **153** (1979) 161.

[35] G. Curci, W. Furmanski, and R. Petronzio, Nucl. Phys. B **175** (1980) 27.

[36] F. M. Dittes and A. V. Radyushkin, Phys. Lett. B **134** (1984) 359.

[37] M. H. Sarmadi, Phys. Lett. B **143** (1984) 471.

[38] S. V. Mikhailov and A. V. Radyushkin, Nucl. Phys. B **254** (1985) 89.

[39] H.-M. Choi and C.-R. Ji, Phys. Rev. D **75** (2007) 034019, hep-ph/0701177.

[40] A. E. Dorokhov, Czech. J. Phys. **56** (2006) F169, hep-ph/0610212.

[41] P. Ball and G. Jones, JHEP **0703** (2007) 069, hep-ph/0702100.

[42] M. Ahmady and R. Sandapen, Phys. Rev. D **87** (2013) 054013, arXiv:1212.4074.

[43] S. J. Brodsky and G. F. de Teramond, Phys. Rev. D **77** (2008) 056007, arXiv:0707.3859.

[44] H. J. Behrend et al. (CELLO Collaboration), Z. Phys. C **49** (1991) 401.

[45] J. Gronberg et al. (CLEO Collaboration), Phys. Rev. D **57** (1998) 33, hep-ex/9707031.

[46] B. Aubert et al. (BaBar Collaboration), Phys. Rev. D **80** (2009) 052002, arXiv:0905.4778.

[47] S. Uehara et al. (Belle Collaboration), Phys. Rev. D **86** (2012) 092007, arXiv:1205.3249.

[48] S. V. Mikhailov, A. V. Pimikov, and N. G. Stefanis, Phys. Rev. D **82** (2010) 054020, arXiv:1006.2936.

[49] V. M. Braun, S. Collins, M. Göckeler, P. Pérez-Rubio, A. Schäfer, et al., Phys. Rev. D **92** 014504 (2015) arXiv:1503.03656.

[50] S. J. Brodsky, F.-G. Cao, and G. F. de Teramond, Phys. Rev. D **84** (2011) 033001, arXiv:1104.3364.

[51] F. M. Dittes and A. V. Radyushkin, Sov. J. Nucl. Phys. **34** (1981) 293.

[52] S. H. Strogatz, Physica D **143** (2000) 1.

[53] J. A. Acebron, L. L. Bonilla, C. J. Perez Vicente, F. Ritort, and R. Spigler, Rev. Mod. Phys. **77** (2005) 137.

[54] Y. Kuramoto, *Chemical Oscillations, Waves and Turbulence*, (Springer Verlag, Berlin, 1984).

[55] S. S. Agaev, V. M. Braun, N. Offen, and F. A Porkert, Phys. Rev. D **86** (2012) 077504, arXiv:1206.3968.

[56] I. C. Cloet and C. D. Roberts, Prog. Part. Nucl. Phys. **77** (2014) 1, arXiv:1310.2651.

[57] H.-M. Choi and C.-R. Ji, Phys. Rev. D **91** (2015) 014018, arXiv:1412.2507.

[58] S. J. Brodsky, G. F. de Teramond, and H. G. Dosch, Few Body Syst. **55** (2014) 407, arXiv:1310.8648.

[59] M. A. Shifman, A. I. Vainshtein, and V. I. Zakharov, Nucl. Phys. B **147** (1979) 385.

[60] C. Shi, L. Chang, C. D. Roberts, S. M. Schmidt, P. C. Tandy, et al., Phys. Lett. B **738** (2014) 512, arXiv:1406.3353.

[61] C. Shi, C. Chen, L. Chang, C. D. Roberts, S. M. Schmidt, et al., arXiv:1504.00689.

[62] N. G. Stefanis, W. Schroers, and H.-C. Kim, Phys. Lett. B **449** (1999) 299, hep-ph/9807298.

[63] N. G. Stefanis, W. Schroers, and H.-C. Kim, Eur. Phys. J. C **18** (2000) 137, hep-ph/0005218.

[64] R. Swarnkar and D. Chakrabarti, Phys. Rev. D **92** 074023 (2015), arXiv:1507.01568.

[65] T. Zhong, X. G. Wu, and T. Huang, arXiv:1510.06924 [hep-ph].

[66] K. Raya, L. Chang, A. Bashir, J. J. Cobos-Martinez, L. X. Gutiérrez-Guerrero, C. D. Roberts, and P. C. Tandy, arXiv:1510.02799 [nucl-th].

[67] N. Brambilla, S. Eidelman, P. Foka, S. Gardner, A. S. Kronfeld, et al., Eur. Phys. J. C **74** (2014) 2981, arXiv:1404.3723.

[68] N. G. Stefanis and M. Bergmann, Phys. Rev. D **47** (1993) 3685, hep-ph/9211250.

[69] M. Bergmann and N. G. Stefanis, Phys. Rev. D **48** (1993) 2990.

[70] M. Bergmann and N. G. Stefanis, Phys. Lett. B **325** (1994) 183, hep-ph/9403209.

[71] N. G. Stefanis and M. Bergmann, Phys. Lett. B **304** (1993) 24, hep-ph/9211251.

[72] Y. Kuramoto and D. Battogtokh, Nonlinear Phenom. Complex Syst. **5** (2002) 380.

[73] D. M. Abrams and S. H. Strogatz, Phys. Rev. Lett. **93** (2004) 174102.